ISSN 1063-7842, Technical Physics, 2019, Vol. 64, No. 2, pp. 236–241. © Pleiades Publishing, Ltd., 2019.
Russian Text © A.V. Kobyakov, I.A. Turpanov, G.S. Patrin, R.Yu. Rudenko, V.I. Yushkov, N.N. Kosyrev, 2019, published in Zhurnal Tekhnicheskoi Fiziki, 2019, Vol. 89, No. 2, pp. 268–273.

PHYSICS OF NANOSTRUCTURES

Structural and Magnetic Properties of the Al_2O_3/Ge-*p*/Al_2O_3/Co System

A. V. Kobyakov[a,b],*, I. A. Turpanov[b], G. S. Patrin[a,b], R. Yu. Rudenko[a,b], V. I. Yushkov[a,b], and N. N. Kosyrev[b,c]

[a] *Siberian Federal University, Krasnoyarsk, 660041 Russia*
[b] *Kirensky Institute of Physics, Federal Research Center Krasnoyarsk Scientific Center, Siberian Branch, Russian Academy of Sciences, Krasnoyarsk, 660036 Russia*
[c] *Krasnoyarsk State Agrarian University (Achinsk Branch), Krasnoyarsk, Krasnoyarsk krai, 662150 Russia*
**e-mail: nanonauka@mail.ru*

Received May 15, 2018

Abstract—The Al_2O_3/Ge-*p*/Al_2O_3/Co system with an Al_2O_3 buffer layer deposited by ion-plasma sputtering has been experimentally investigated. The dependences of the magnetic properties of cobalt on the rate of its deposition by ion-plasma sputtering and rate of deposition of preceding layers have been established. It is shown that the technique used to obtain buffer layers can significantly reduce the surface roughness of the next layers. The obtained buffer layers can be used as artificial substrates for growing heterostructures with tunnel junctions.

DOI: 10.1134/S1063784219020087

INTRODUCTION

Recently, a study of the mechanisms responsible for the formation of physical properties of ferromagnetic metal/insulator/semiconductor (FMM/I/SC) thin-film structures has been of great importance. The transport properties of the FMM/SC structures can be controlled by manipulating the electron spin states [1–3]. For instance, it becomes possible to store, process, and transmit data in a single electronic chip. A highly promising research direction is the giant magnetoresistance effect.

In particular, it was demonstrated [4] that the presence of a transition layer affects the magnetic behavior and magnetoresistive effect in the Co/Ge FMM/SC bilayer. Such an interface between layers, depending on the deposition rate and substrate temperature, can be fairly diffuse, since it is strongly affected by synthesis conditions, structure roughness, and, consequently, the presence of several magnetic phases. The transition layer can reduce the magnetic anisotropy; i.e., there is competition between the contributions of the transition and cobalt layers.

Another promising direction is forming thin dielectric (oxide or other) spacers. The aluminum oxide has high application potential as a dielectric gate of field-effect transistors [5, 6], an antireflection layer for optical mirrors of semiconductor lasers [7], etc. [8, 9]. Embedding of insulating layers in an FMM/SC structure can lead to the formation of tunnel structures.

Dai et al. [10] showed that in an FMM/SiO_2/Si system with CoSi or FeSi as a ferromagnetic metal, the resistance undergoes a sharp transition in a very thin metallic layer at the film/silicon substrate interface at 250–270 K [10]. Here, a certain role is played by the ferromagnetic state of the metallic layer, which is very unusual for spin-dependent electron tunneling through the SiO_2/*p*-Si interface. These features were explained by the existence of a Schottky barrier in the metal/insulator/semiconductor system.

Therefore, it is no surprise that the magnetic tunnel structures and thin-film structures with tunnel junctions where a current flows along the interfaces attract close attention of research [11–15].

Meanwhile, forming high-quality interfaces between the structural layers with required properties is quite a challenge.

The deposition of aluminum oxide thin films by ion-plasma sputtering has been understudied. The well-proven techniques for synthesizing Al_2O_3 are electron beam evaporation [8] and magnetron sputtering [16]. The condensation of alumina is accompanied by phase transformations, the degree of completion of which and, consequently, the operational properties of the material depend on the condensation method

Table 1. Rates and thicknesses of Al_2O_3/Ge-*p*/Al_2O_3/Co structural layers

Film type	Al_2O_3 deposition rate/thickness	Ge-*p* deposition rate/thickness	Al_2O_3 deposition rate/thickness	Co deposition rate/thickness
1	0.05 nm/min/33 nm	2.4 nm/min/54 nm	0.05 nm/min/4.7 nm	1.2 nm/min/104.7 nm
2	0.55 nm/min/220 nm	14.4 nm/min/31 nm	0.55 nm/min/16 nm	7.2 nm/min/106 nm

used, substrate temperature, film thickness, purity of alumina, and other factors.

Thus, in such systems, of primary importance is to study the effect of interfaces between layers on the formation of a structure and its physical, including magnetic, properties and spin-dependent transport in it. As objects of study, Al_2O_3/Ge-*p*/Al_2O_3/Co samples were chosen. The semiconductor was boron-doped germanium with *p*-type conductivity. The material of the insulating layer between the substrate and Ge-*p* was Al_2O_3, since it exhibits unique electrical and optical properties, high hardness, heat stability, chemical inertness, and heat-protective properties.

EXPERIMENTAL

Al_2O_3/Ge-*p*/Al_2O_3/Co structures were deposited by ion-plasma sputtering under a base pressure of $P =$ 0.1 Pa in argon atmosphere. The substrate material was Si(001) pre-cleaned by ion-plasma etching in a working chamber right before sputtering. The deposition was performed onto a rotating substrate with a temperature of $T \approx 373$ K.

The samples of two types were obtained at deposition rates different by an order of magnitude for Al_2O_3 and by a factor of 5 for Ge-*p* and Co. The average rates and thicknesses for the obtained structures are given in Table 1.

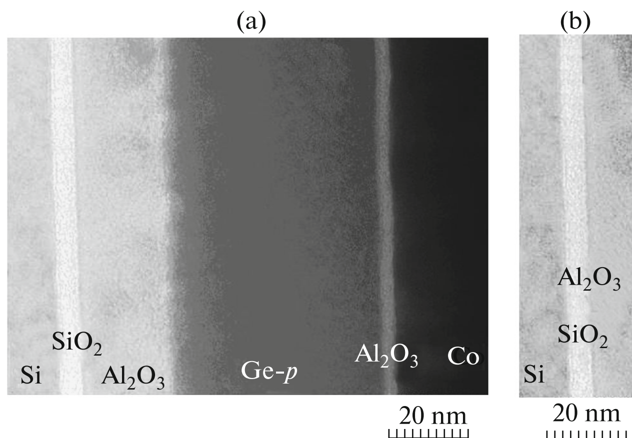

Fig. 1. TEM images of (a) Al_2O_3/Ge-*p*/Al_2O_3/Co films and (b) substrate/Al_2O_3 interface for type-I samples.

In addition, to analyze the obtained parameters of the Al_2O_3/Ge-*p*/Al_2O_3/Co multilayers, pure cobalt films were deposited onto a similar substrate precleaned by ion-plasma etching:

Type-I samples: a deposition rate of 1.2 nm/min and thickness of ~100 nm;

Type-II samples: a deposition rate of 7.2 nm/min and a thickness of ~100 nm.

Cross-sectional transmission electron microscopy (TEM) images of the structure were obtained on a Hitachi HT7700 microscope. The images were used to determine the averaged thicknesses. The film surface structure was examined on a Veeco Multi-Mode atomic force microscope (AFM) at a resolution of 1 nm. The magnetic data were obtained on a SQUID magnetometer (Quantum Design MPMS_XL) operating in the temperature range of $T = 4.2–300$ K in magnetic fields of $H \leq 800$ Oe in the in-plane magnetic field geometry. Before each measurement, the film was first placed in a demagnetizer and then cooled in zero magnetic field (ZFC mode). In addition, magneto-optical Kerr effect (NanoMOKE-2) measurements were performed.

RESULTS AND DISCUSSION

Figures 1a and 2a show cross-sectional TEM images of the structure. It can be seen that after ion-plasma etching of the substrate, solid and smooth (a roughness of about 1–2 nm) interfaces formed between the substrate and Al_2O_3 layer in the films of

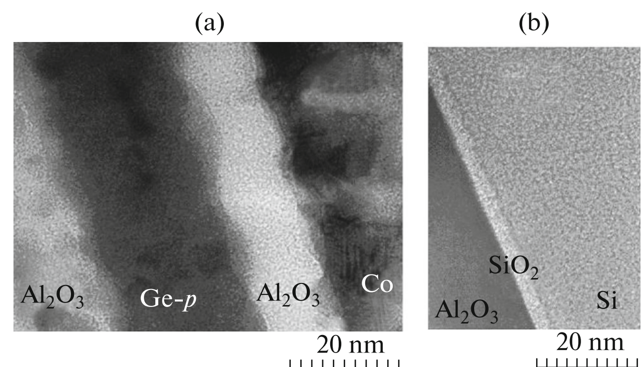

Fig. 2. TEM images of (a) Al_2O_3/Ge-*p*/Al_2O_3/Co films and (b) substrate/Al_2O_3 interface for type-II samples.

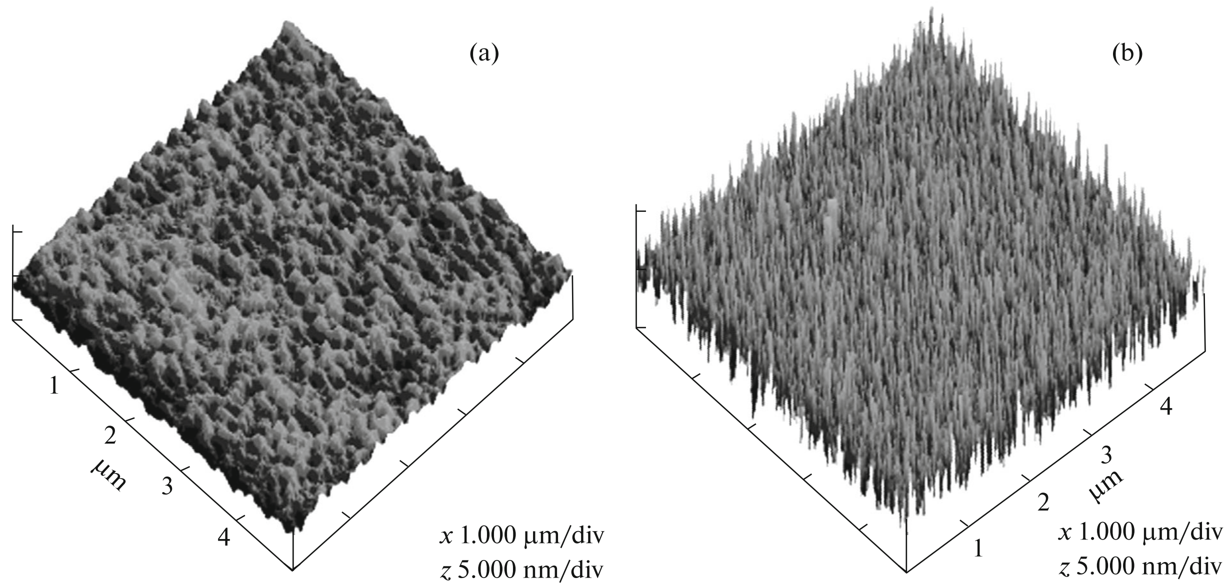

Fig. 3. Atomic force microscopy of Al_2O_3/Ge-*p*/Al_2O_3/Co films. (a) Low deposition rate (type-I samples) and (b) high deposition rate (type-II samples).

both types (Figs. 1b, 2b). A (4–5)-nm-thick silicon oxide layer was observed on the substrate. Then, in type-I films (Fig. 1a), the roughness of interfaces between the subsequent layers slightly changes and, in type-II films, increases very sharply (Fig. 2b).

The morphology of Al_2O_3/Ge-*p*/Al_2O_3/Co films was studied by atomic force microscopy. Figure 3 shows the results for just-deposited type-I and type-II films.

In addition, roughness parameters of the top cobalt layer for all pure cobalt and Al_2O_3/Ge-*p*/Al_2O_3/Co multilayer samples were determined. The roughness parameters of type-I and type-II films for some samples are given in Table 2. The analysis of these data showed that the roughness of pure cobalt film halves with decreasing deposition rate. At the same time, in the Al_2O_3/Ge-*p*/Al_2O_3/Co multilayer film, the roughness of the upper cobalt layer decreases by a factor of 3–5 with a decrease in the rate of deposition of each layer. Thus, the rate of deposition of intermediate layers affects the upper layer roughness.

Images of the magnetization distribution in the investigated films were obtained on an atomic force microscope using magnetic cantilevers. Figure 4 shows magnetic contrast images of type-I pure cobalt and Al_2O_3/Ge-*p*/Al_2O_3/Co films. Using the magnetic contrast technique for determining the surface roughness, one can estimate the degree of inhomogeneity of the sample magnetic moment.

Table 3 gives magnetic roughness parameters for the same samples as in Table 2.

It can be seen in Fig. 4 that the magnetic surface of the type-I multilayer film, in contrast to the pure cobalt film, is finer, regardless of the deposition rate used. According to the data from Table 3, we may conclude that the magnetic roughness of Al_2O_3/Ge-*p*/Al_2O_3/Co multilayer structures decrease by a factor of 3–5 at a lower deposition rate. This can be explained by a change in the magnetic phase composition and a more uniform distribution of materials during deposition. The average grain size for Al_2O_3/Ge-*p*/Al_2O_3/Co structures was found to be $d \approx 0.84$ nm.

Table 2. Roughness parameters of the films for type-I and II Al_2O_3/Ge-*p*/Al_2O_3/Co and Co films

Averaged parameter	Type I		Type II	
	Al_2O_3/Ge-*p*/Al_2O_3/Co	Co	Al_2O_3/Ge-*p*/Al_2O_3/Co	Co
Rms (Rq)	0.415 nm	2.850 nm	1.226 nm	4.589 nm
Mean rougness (Ra)	0.329 nm	2.000 nm	0.957 nm	2.835 nm
Max height (Rmax)	3.296 nm	27.115 nm	17.168 nm	30.616 nm
10 pt mean (Rz)	3.025 nm	15.970 nm	12.864 nm	20.453 nm

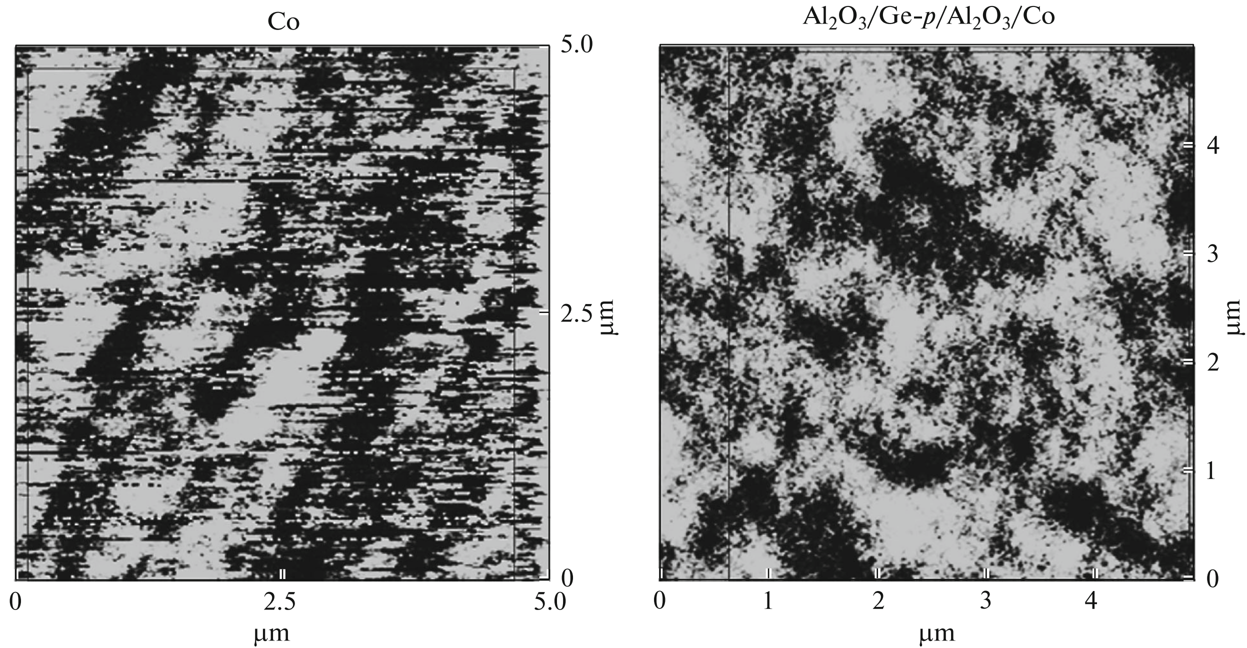

Fig. 4. Magnetic roughness of type-I Co and Al_2O_3/Ge-*p*/Al_2O_3/Co samples.

The magnetic measurements on a SQUID magnetometer yielded hysteresis loops for type-I and type-II Al_2O_3/Ge-*p*/Al_2O_3/Co layers (Fig. 5a) and for type-I and type-II pure cobalt layer without sublayers (Fig. 6).

Analysis of the loops showed that the room-temperature coercivity of the pure cobalt layer (Fig. 5) at low deposition rates (type I) is about 50 Oe and increases to 200 Oe as the temperature decreases to 4 K. At high rates (type II), the room-temperature coercivity is about 70 Oe and increases to 250 Oe with a decrease in temperature to 4 K.

In the Al_2O_3/Ge-*p*/Al_2O_3/Co system (Fig. 6a), the room-temperature coercivity at low rates (type I) is about 100 Oe; with a decrease in temperature to 4 K, it attains 160 Oe. At high rates (type II, Fig. 6b), the room-temperature coercivity is about 160 Oe; with a decrease in temperature to 4 K, it increases to 280 Oe.

As is known [17], with an increase in the cobalt deposition rate, the average grain size of Co films increases and the surface relief changes: it becomes less uniform, as can be seen from microscopy and magnetic measurement data. However, the temperature dependences of coercivity (Fig. 6b) for the Al_2O_3/Ge-*p*/Al_2O_3/Co system show different coercivity variation rates upon temperature variation (the curve slope).

It can be seen that at the same deposition rate of pure cobalt and cobalt in the Al_2O_3/Ge-*p*/Al_2O_3/Co system, the coercivities differ twofold or more (Fig. 6b). As is known, with a decrease in the cobalt deposition rate, the hexagonal phase fraction decreases and additional phases arise. Thus, the difference between coercivities of the samples and steepness of the temperature dependences of the coercivity can be related to the

Table 3. Magnetic roughness parameters of the films for type-I and II Al_2O_3/Ge-*p*/Al_2O_3/Co and Co films

Averaged parameter	Type I		Type II	
	Al_2O_3/Ge-*p*/Al_2O_3/Co	Co	Al_2O_3/Ge-*p*/Al_2O_3/Co	Co
Rms (Rq)	0.328 nm	0.816 nm	0.988 nm	1.072 nm
Mean rougness (Ra)	0.262 nm	0.599 nm	0.672 nm	0.816 nm
Max height (Rmax)	2.913 nm	12.813 nm	36.106 nm	14.383 nm
10 pt mean (Rz)	2.519 nm	11.583 nm	21.480 nm	12.508 nm

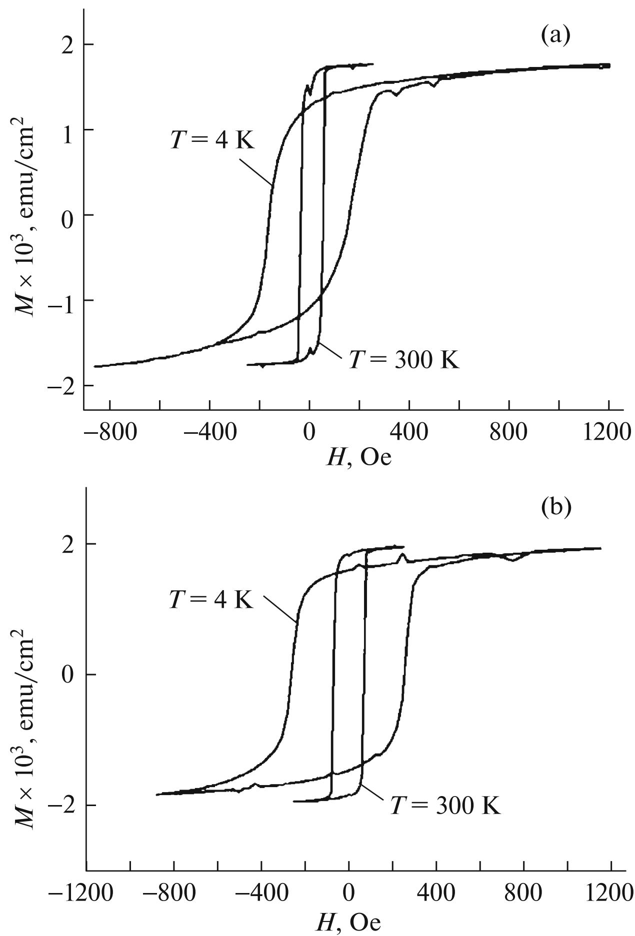

Fig. 5. Hysteresis loops for the pure cobalt layer at $T = 300$ and 4 K. (a) Type-I (slow) and (b) type-II samples (fast).

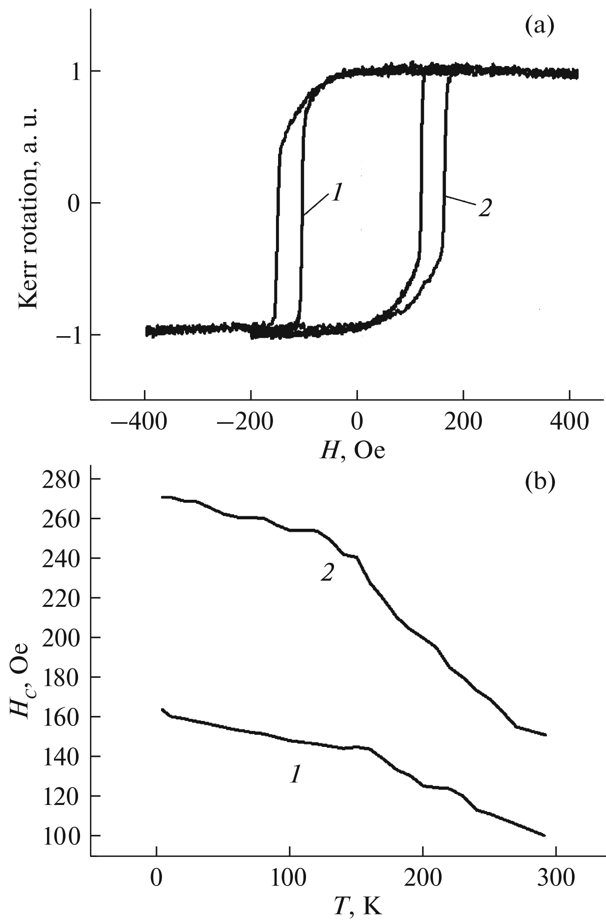

Fig. 6. (a) Hysteresis loops at $T = 300$ K and (b) temperature dependence of the coercivity for type-I and type-II Al_2O_3/Ge–*p*/Al_2O_3/Co samples.

rate of deposition of cobalt sublayers in the system, since the surface relief depends on the rate of deposition of the preceding layer and, consequently, affects the structure of the following layers. Specifically, the change in coercivity of Al_2O_3/Ge-*p*/Al_2O_3/Co systems is related to the anisotropy at the interface.

CONCLUSIONS

The study of the Al_2O_3/Ge-*p*/Al_2O_3/Co system showed the dependence of the magnetic properties of cobalt on the rate of its deposition by ion-plasma sputtering and the rate of deposition of the preceding layers. Reducing the rate of layer deposition in a multilayer structure makes it possible to reduce the roughness of interfaces between adjacent layers and average grain size, as well as reduce and stabilize the coercivity. This can be important for designing spintronic devices, e.g., magnetic sensors. For a more detailed description, it is necessary to consider the interfacial structure [18], since the interface thickness is only a few nanometers and new phases are formed in it.

ACKNOWLEDGMENTS

This study was supported by the Russian Foundation for Basic Research, project no. 18-02-00161-a.

REFERENCES

1. A. Fert, Phys.-Usp. **51**, 1336 (2008).
2. S. Dushenko, M. Koike, Y. Ando, T. Shinjo, M. Myronov, and M. Shiraishi, Phys. Rev. Lett. **114**, 196602 (2015).
3. Y. Song, O. Chalaev, and H. Dery, Phys. Rev. Lett. **113**, 167201 (2014).
4. G. S. Patrin, I. A. Turpanov, K. G. Patrin, E. Alekseichik, V. I. Yuchkov, and A. V. Kobyakov, Bull. Russ. Acad. Sci.: Phys. **78**, 26 (2014).
5. H. C. Lin, P. D. Ye, and G. D. Wilk, Appl. Phys. Lett. **87**, 182904 (2005).
6. Y. Xuan, Y. Q. Wu, H. C. Lin, T. Shen, and D. Ye. Peide, IEEE Electron Device Lett. **28**, 935 (2007).
7. P. V. Seredin, D. L. Goloschapov, A. N. Lukin, A. S. Len'shin, A. D. Bondarev, I. N. Arsent'ev, L. S. Vavilova, and I. S. Tarasov, Semiconductors **48**, 1527 (2014).

8. A. L. Borisova, D. I. Adeeva, and V. N. Sladkova, Avtom. Svarka, No. 9, 26 (1997).
9. L. A. Krushinskaya and Ya. A. Stel'makh, Vopr. At. Nauki Tekh., Ser.: Vak., Chist. Mater., Sverkhprovodn., No. 19, 92 (2011).
10. J. Dai, L. Spinu, K.-Y. Wang, L. Malkinski, and J. Tang, J. Phys. D: Appl. Phys. **33**, L65 (2000).
11. N. V. Volkov, A. S. Tarasov, A. O. Gustajcev, O. N. Volkova, S. N. Varnakov, and S. G. Ovchinnikov, Trans. Nonferrous Met. Soc. China **24**, 3158 (2014).
12. N. V. Volkov, A. S. Tarasov, E. V. Eremin, S. N. Varnakov, S. G. Ovchinnikov, and S. M. Zharkov, J. Appl. Phys. **109**, 123924 (2011).
13. Y. Song and H. Dery, Phys. Rev. Lett. **113**, 047205 (2014).
14. O. Txoperena, Y. Song, L. Qing, M. Gobbi, L. E. Hueso, H. Dery, and F. Casanova, Phys. Rev. Lett. **113**, 146601 (2014).
15. K. Ando, S. Takahashi, J. Ieda, Y. Kajiwara, H. Nakayama, T. Yoshino, K. Harii, Y. Fujikawa, M. Matsuo, and S. Maekawa, J. Appl. Phys. **109**, 103913 (2011).
16. V. V. Teslenko-Ponomarenko, Vopr. At. Nauki Tekh., Ser.: Vak., Chist. Mater., Sverkhprovodn., No. 13, 175 (2003).
17. G. S. Patrin, I. A. Turpanov, A. V. Kobyakov, D. A. Velikanov, K. G. Patrin, L. A. Li, V. K. Mal'tsev, S. M. Zharkov, and V. I. Yushkov, Phys. Solid State **56**, 302 (2014).
18. G. S. Patrin, A. V. Kobyakov, I. A. Turpanov, K. G. Patrin, and M. Rautskii, Phys. Solid State **58**, 1034 (2017).

Translated by E. Bondareva